Time-Encoded Bio-Fluorochromic Supramolecular Co-Assembly for Rewritable Security Printing

Z. Gao *et al.*

Supplementary Methods

Reagents and reactants: 9,10-diiodoanthracene,[1] compound **4**,[2] and compound **5** [3] (see supplementary Figure 1) were synthesized according to the previously reported literatures. Other reagents and solvents used in the experiments were purchased from the commercial sources without further purification.

*Synthesis of compound **3***: N-Boc-1,3-propanediamine (696 mg, 4.00 mmol), compound **4** (400 mg, 1.52 mmol)， EDC (1-(3-Dimethylaminopropyl)-3-ethylcarbodiimide hydrochloride) (560 mg, 2.92 mmol) and DMAP (4-dimethylaminopyridine) (720 mg, 5.9 mmol) were mixed in 20 mL of CH_2Cl_2. After stirring at room temperature for 12 hours, the mixture was extracted with H_2O/CH_2Cl_2 for three times. The combined organic extracts were dried over anhydrous Na_2SO_4, and the solvent was removed with a rotary evaporator. The residue was purified by flash column chromatography (petroleum ether/CH_2Cl_2, 5 : 1 *v*/*v* as the eluent) to afford the esterification product (752 mg, 87 %). It was then treated with tetrabutylammonium hydroxide (647 mg, 2.48 mmol) in 20 mL of THF at room temperature for 6 hours. After the deprotection reaction, the solvent was removed in vacuo, and the residue was extracted with H_2O/CH_2Cl_2. The combined organic extracts were dried over anhydrous Na_2SO_4 and evaporated with a rotary evaporator. The residue was purified by flash column chromatography (petroleum ether/CH_2Cl_2, 5 : 1 *v*/*v* as the eluent) to afford compound **3** as a white solid (566 mg, 86 %). ^{1}H NMR (400 MHz, $CDCl_3$, supplementary Figure 2) δ (ppm): 8.26 (s, 1H), 8.16 (d, J = 18.9 Hz, 2H), 7.41 (s, 2H), 4.97 (s, 2H), 3.52 (dd, J = 11.9, 6.0 Hz, 4H), 3.29–3.21 (m, 4H), 3.15 (s, 1H), 1.77–1.70 (m, 4H), 1.44 (s, 18H). ^{13}C NMR (101 MHz, $CDCl_3$, supplementary Figure 3) δ (ppm): 166.02, 156.90, 136.42, 135.01, 133.62, 123.31, 82.00, 79.62, 78.88, 37.17, 36.48, 29.90, 28.37. MALDI-TOF-MS *m*/*z*: $[M+H]^+$, $C_{26}H_{39}N_4O_6$, calculated 503.2870; found 503.2913.(supplementary Figure 4).

*Synthesis of compound **2***: 9,10-diiodoanthracene (97.0 mg, 0.23 mmol), compound **3** (258 mg, 0.51 mmol), $Pd(PPh_3)_2Cl_2$ (30mg, 0.04 mmol) and CuI (25.0 mg, 0.13 mmol)

were mixed in 20 mL of TEA under nitrogen atmosphere. After stirring at 75 ºC for 12 hours, the reaction mixture was evaporated to remove the solvent, and the residue was extracted with H_2O/CH_2Cl_2 for three times. The combined organic extracts were dried over anhydrous Na_2SO_4, and the solvent was removed with a rotary evaporator. The residue was purified by flash column chromatography (petroleum ether/CH_2Cl_2, 5 : 1 *v*/*v* as the eluent) to afford compound **2** as a yellow solid (153 mg, 57 %). ^{1}H NMR (400 MHz, DMSO-d_6, supplementary Figure 5) δ (ppm): 8.85–8.71 (m, 8H), 8.44 (s, 4H), 8.40 (s, 2H), 7.88 (s, 4H), 6.87 (s, 4H), 3.02 (d, J = 6.1 Hz, 8H), 1.75–1.63 (m, 8H), 1.38 (s, 36H). ^{13}C NMR (101 MHz, $CDCl_3$, supplementary Figure 6) δ (ppm): 166.21, 165.65, 156.83, 136.35, 134.93, 133.54, 133.23, 125.24, 123.63, 123.14, 123.02, 81.93, 79.55, 78.92, 37.21, 36.60, 29.73, 28.33. MALDI-TOF-MS *m*/*z*: $[M+H]^+$, $C_{66}H_{83}N_8O_{12}$, calculated 1179.6130; found 1179.6535. (supplementary Figure 7).

*Synthesis of monomer **1***: A concentrated HCl solution was added into a dioxane (10 mL) solution of compound **2** (153 mg, 0.13 mmol) with vigorous stirring at 0 ºC under N_2 atmosphere. The mixture was allowed to warm slowly to room temperature and stirred for 24 h. The yellow precipitation was then washed with dioxane for multiple times, and dry to obtain monomer **1** as a yellow solid (105 mg, 87%). ^{1}H NMR (400 MHz, DMSO-d_6, supplementary Figure 8) δ (ppm): 9.11 (t, J = 5.5 Hz, 4H), 8.80 (dd, J = 6.6, 3.3 Hz, 4H), 8.55 (s, 2H), 8.53 (s, 4H), 7.92 (s, 8H), 7.88 (dd, J = 6.7, 3.2 Hz, 4H), 3.47–3.38 (m, 8H), 2.91 (d, J = 6.4 Hz, 8H), 1.95–1.83 (m, 8H). ^{13}C NMR (101 MHz, DMSO-d_6, supplementary Figure 9) δ (ppm): 168.34, 135.65, 133.97, 132.48, 129.13, 127.90, 127.48, 124.76, 118.60, 102.35, 89.00, 38.31, 38.08, 28.19. MALDI-TOF-MS *m*/*z*: $[M–4Cl]^{4+}$, $C_{46}H_{54}N_8O_4$, calculated 195.6062; found 195.6058. (supplementary Figure 10).

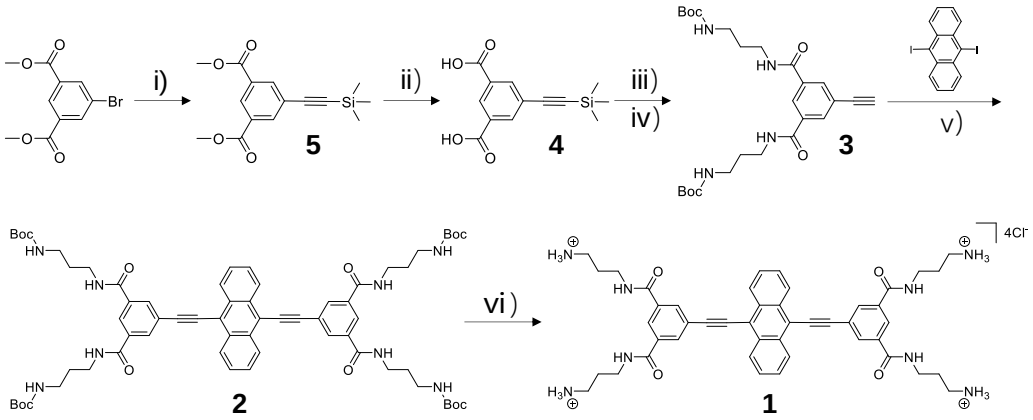

Supplementary Figure 1. Synthetic routes to the targeted monomer 1. i) $Pd(PPh_3)_2Cl_2$, CuI, trimethylsilylacetylene, THF; ii) NaOH, MeOH; iii) EDC, DMAP, CH_2Cl_2; iv) tetrabutylammonium hydroxide, THF; v) $Pd(PPh_3)_2Cl_2$, CuI, TEA; vi) HCl, dioxane, acetone.

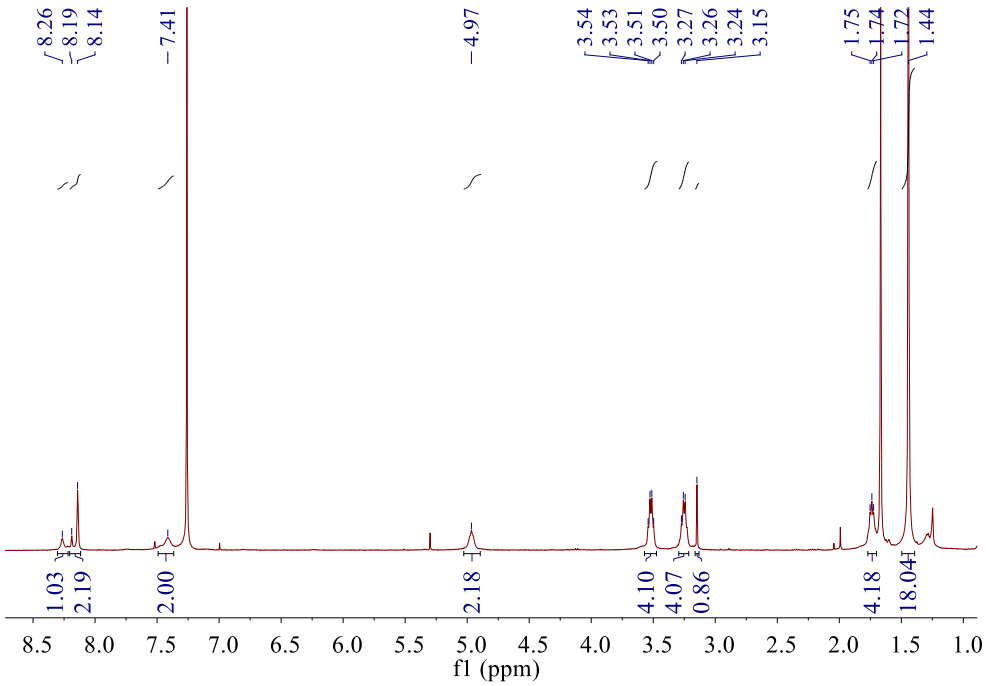

Supplementary Figure 2. ^1H NMR spectrum (400 MHz, $CDCl_3$, 298 K) of compound **3**.

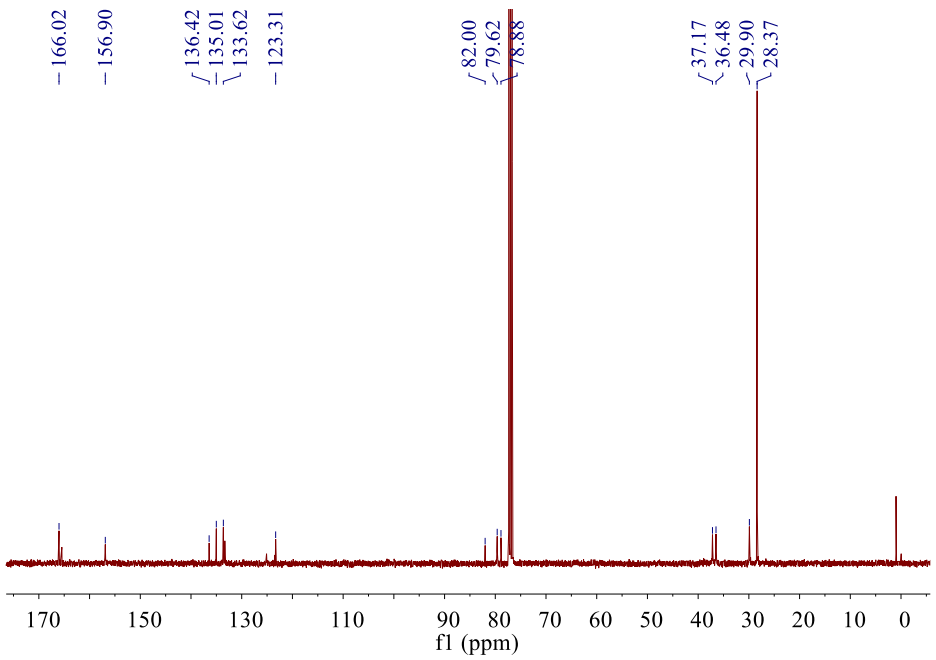

Supplementary Figure 3. ^{13}C NMR spectrum (101 MHz, $CDCl_3$, 298 K) of compound **3**.

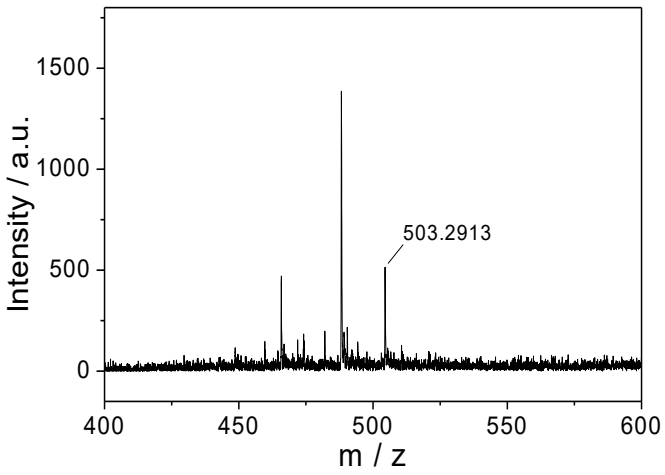

Supplementary Figure 4. MALDI-TOF-MS spectrum of compound **3**.

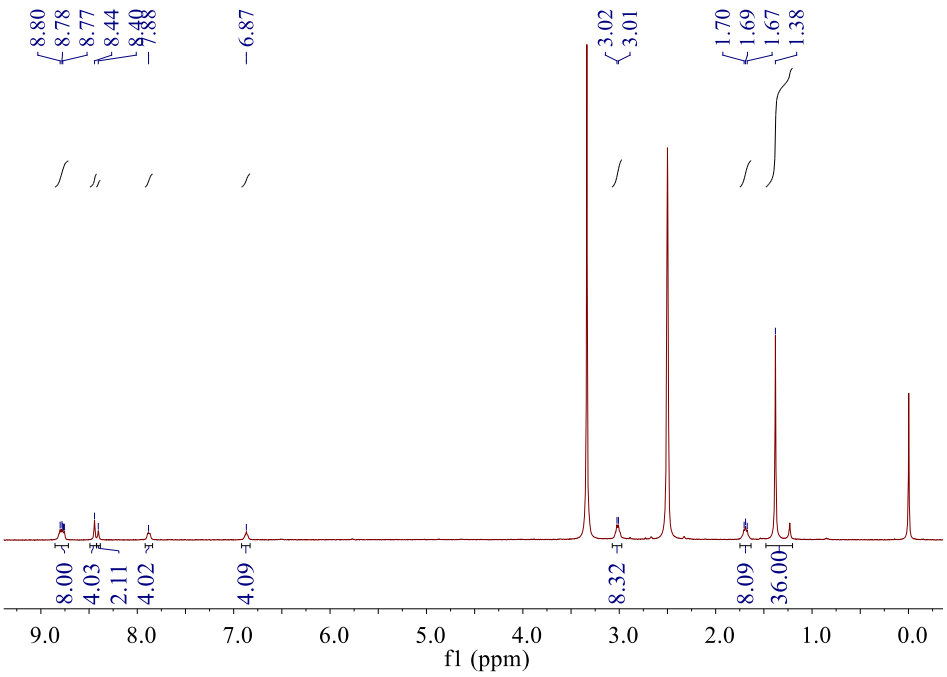

Supplementary Figure 5. ^{1}H NMR spectrum (400 MHz, DMSO-d_6, 298 K) of compound **2**.

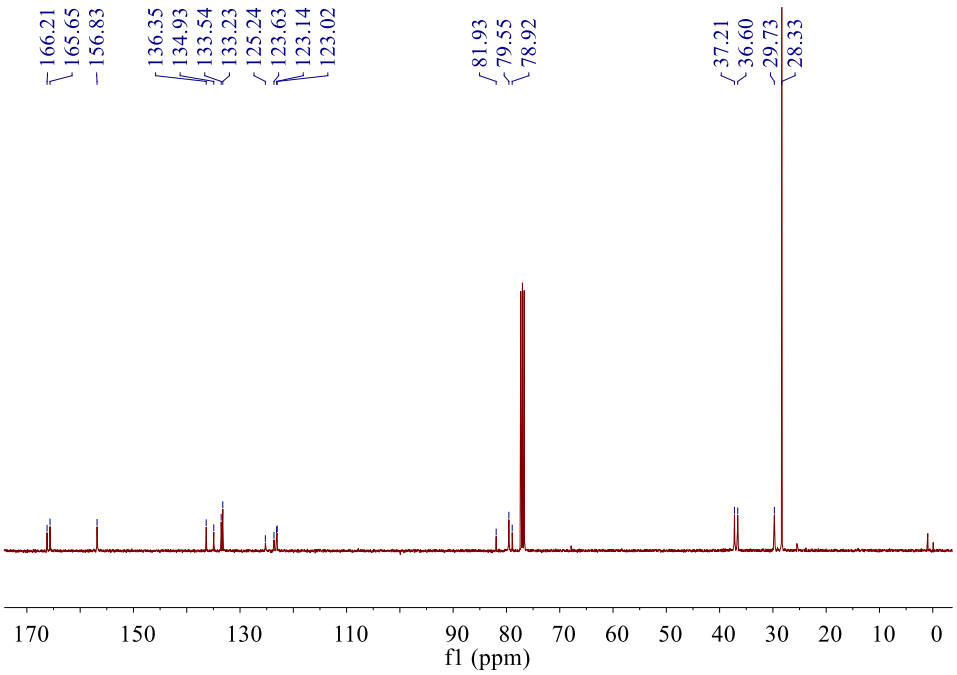

Supplementary Figure 6. ^{13}C NMR spectrum (101 MHz, $CDCl_3$, 298 K) of compound **2**.

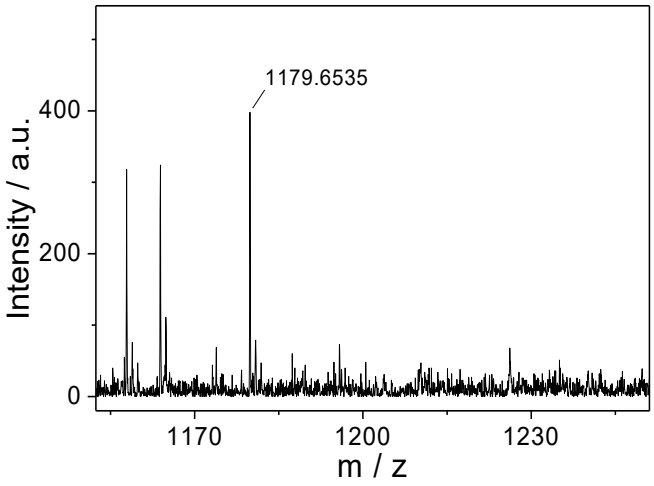

Supplementary Figure 7. MALDI-TOF-MS spectrum of compound **2**.

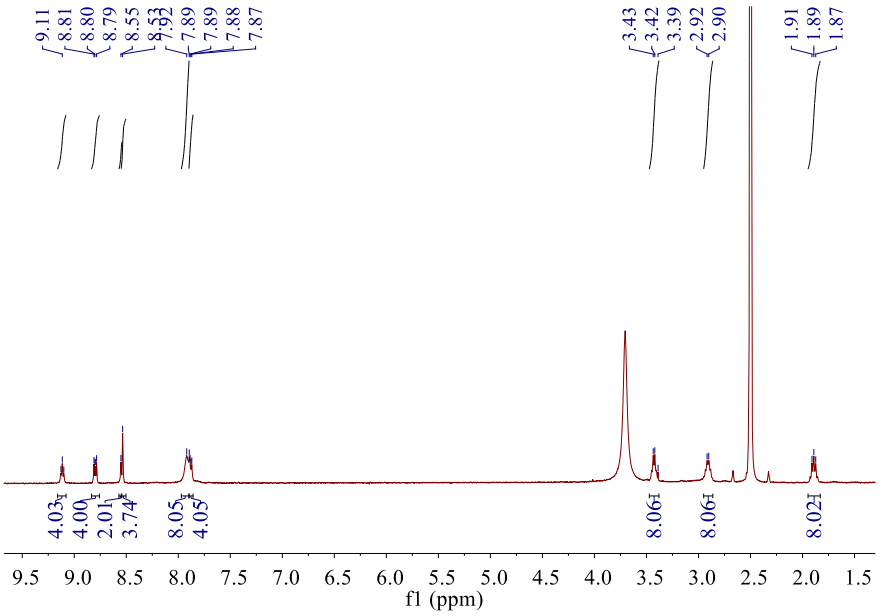

Supplementary Figure 8. ^{1}H NMR spectrum (400 MHz, DMSO-d_6, 298 K) of monomer **1**.

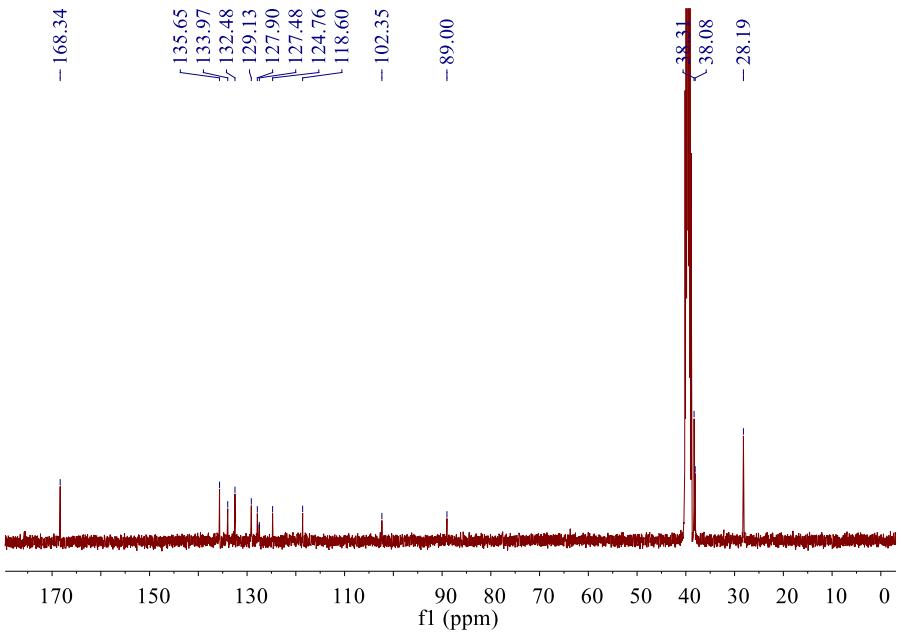

Supplementary Figure 9. ^{13}C NMR spectrum (101 MHz, DMSO-d_6, 298 K) of monomer **1**.

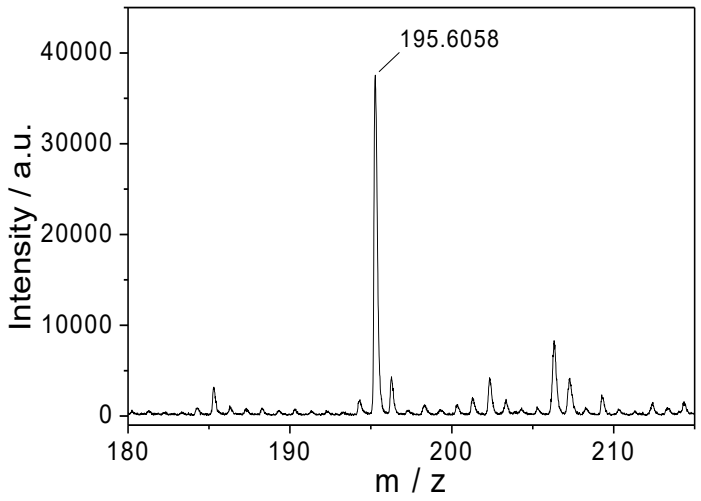

Supplementary Figure 10. MALDI-TOF-MS spectrum of monomer **1**.

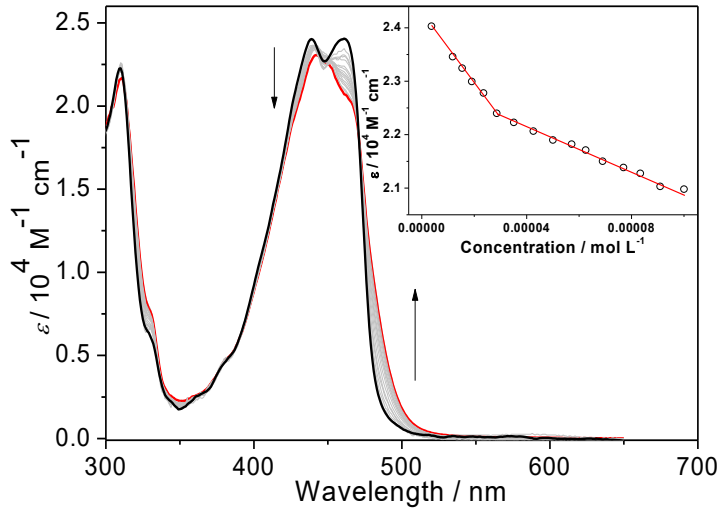

Supplementary Figure 11. Concentration-dependent UV–Vis absorption spectra of **1** in aqueous solution from 4.0×10^{-6} M to 1.0×10^{-4} M. Inset: the plot of absorbance intensity of **1** at 460 nm *versus* concentration. Two distinctive isosbestic points at 471 and 375 nm are observed in the concentration-dependent UV–Vis absorption spectra, which suggests the transition from molecularly dissolved state to self-assembled state. The critical aggregation concentration value of **1** is determined to be 2.9×10^{-5} M, on the basis of an apparent slope transition point of ε at 460nm *versus* concentration.

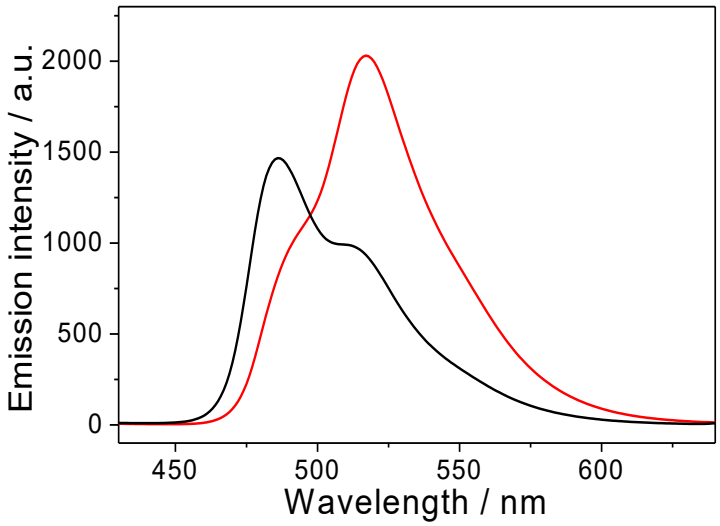

Supplementary Figure 12. Fluorescence spectra of **1** in aqueous solution (black line: 4.0×10^{-6} M, red line: 1.0×10^{-4} M). λ_{ex} = 320 nm. Upon increasing the concentration of **1**, the maximum emission band turns from 484 nm to 517 nm. The red-shifted fluorescent band indicates that **1** possesses the self-assembly capability in aqueous solution.

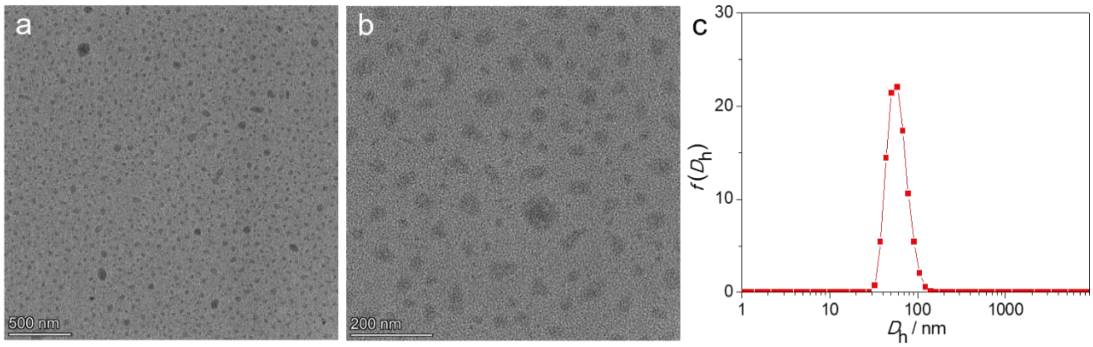

Supplementary Figure 13. (a)–(b) TEM images by drop-casting of **1** (2.0×10^{-4} M) on the copper grids; (c) DLS measurement of **1** in aqueous solution (1.0×10^{-4} M, 298 K). DLS and TEM measurements reveal that **1** can self-assemble into nano-micelles (~60 nm DLS hydrodynamic diameter) in aqueous solution.

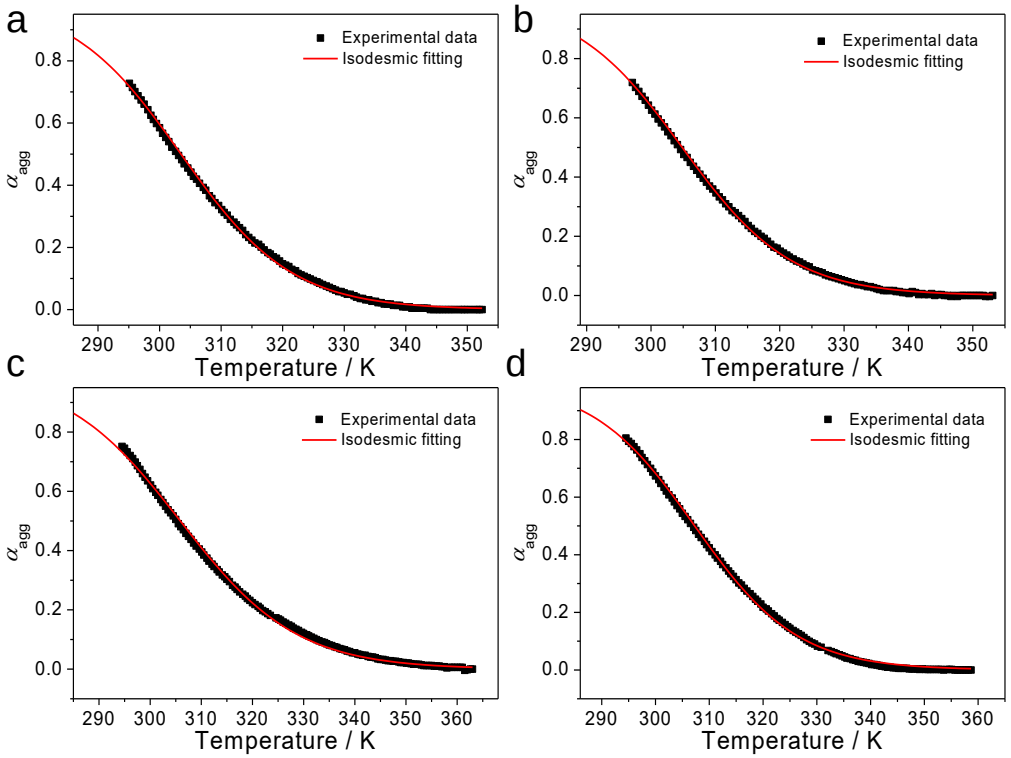

Supplementary Figure 14. Temperature-dependent UV–Vis absorption spectra of **1** in aqueous solution: (a) 0.8×10^{-4} M; (b) 1.0×10^{-4} M; (c) 1.2×10^{-4} M; (d) 1.4×10^{-4} M. The normalized melting curves at λ = 490 nm display sigmoidal curves, which are characteristic for the isodesmic assembling mechanism. Non-linear fitting of the normalized curve affords the corresponding thermodynamic parameters, as shown in Table S1.

Supplementary Table 1. Thermodynamic parameters of the self-assembly process of **1** in aqueous solution, obtained by fitting the temperature-dependent UV–Vis absorption data

Concentration [M]	T_m [a)] [K]	ΔH [b)] [kJ mol^{-1}]
0.8×10^{-4}	303.5	–93.8
1.0×10^{-4}	304.8	–100.9
1.2×10^{-4}	305.9	–85.7
1.4×10^{-4}	307.3	–90.7

[a)]Melting temperature at which α_{agg} is 0.5; [b)]Enthalpy release upon aggregation.

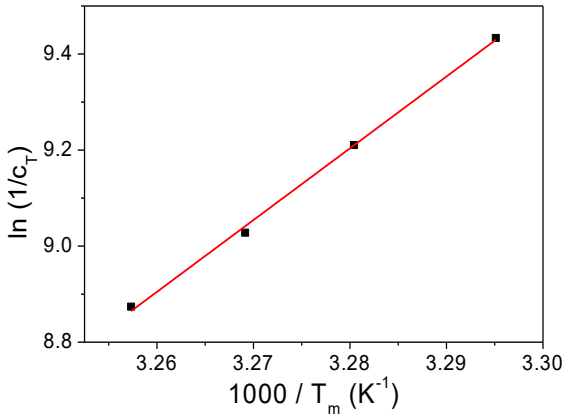

Supplementary Figure 15. Van't Hoff plots of **1**. The red line denotes the respective linear fitting curve. According to the Van't Hoff plot, ΔG of the self-assembly process of **1** is calculated to be –25.7 kJ mol^{-1} at 298 K.

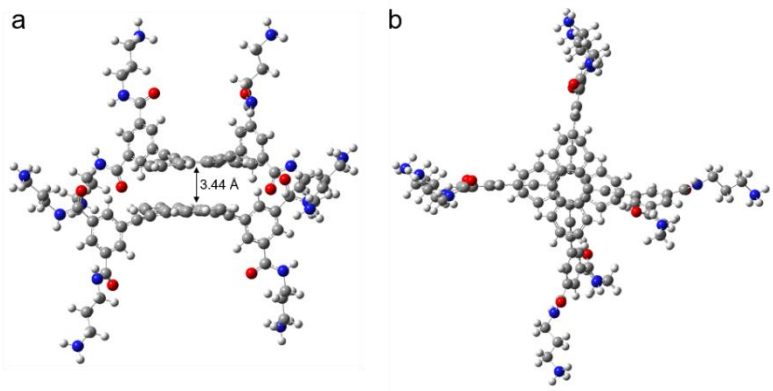

Supplementary Figure 16. Optimized geometries of dimeric structures of **1** at (a) front view and (b) top view, on the basis of DFT calculations at the level of B3LYP/6-31G(d). As can be seen from the front and top views of the dimeric structures **1**, the distance of two anthracene cores is 3.44 Å, indicative of the existence of intermolecular π–π stacking in the self-assembled structures.

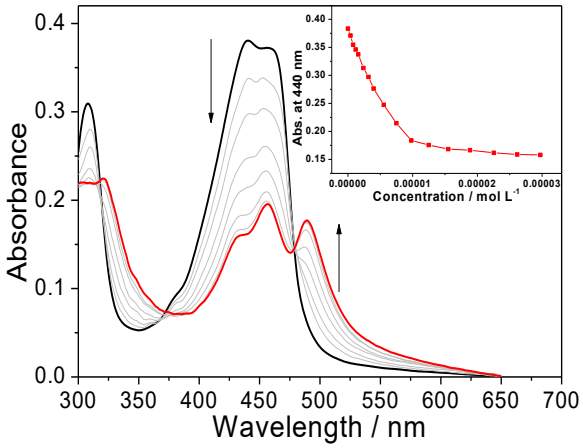

Supplementary Figure 17. UV–Vis spectra variations upon gradual addition of ATP into **1** (*c* = 2.0 × 10^{-5} M). Inset: the absorbance intensity changes at λ = 440 nm.

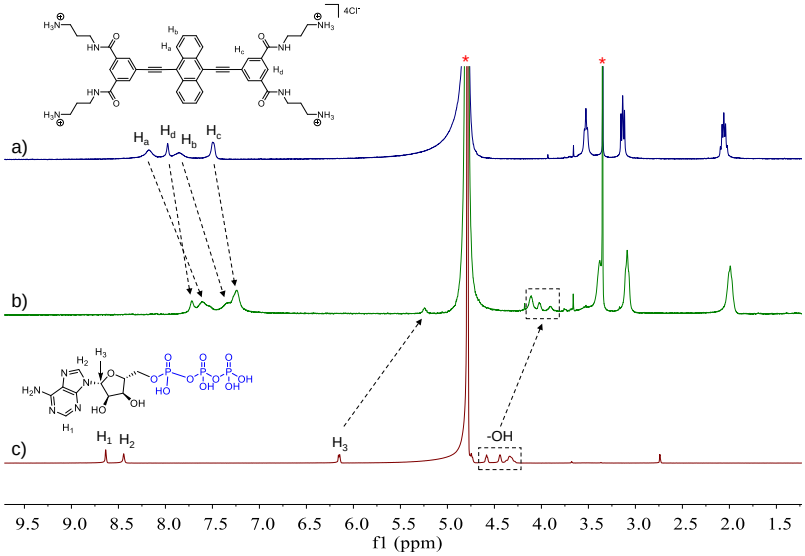

Supplementary Figure 18. Partial ^{1}H NMR spectra (300 MHz, 298 K, 2.00 mM) of a) **1**, b) **1**/ATP, and c) ATP in D_2O. As compared to the individual species, upfield ^{1}H NMR resonances can be observed for an equimolar mixture of **1** and ATP (Δδ = 0.57, 0.52, 0.25, and 0.26 for $H_{a–d}$ on **1**, and 0.91 ppm for H_3 on ATP, respectively), accompanying with the broadened signals.

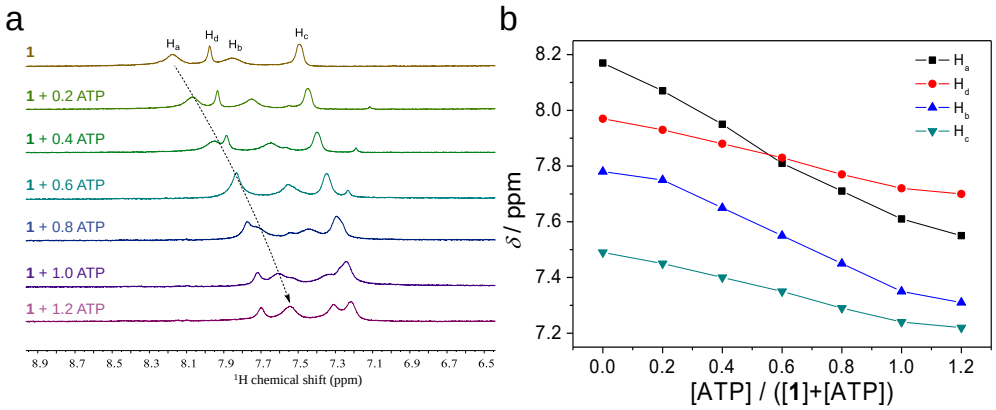

Supplementary Figure 19. (a) Partial ^{1}H NMR spectra (300 MHz, 298 K, 2.00 mM): **1** in D_2O at the presence of 0–1.2 equiv of ATP. The arrow shows the gradual upfield shifting of the H_a proton. (b) $H_{a–d}$ resonances change *versus* the molar ratio of **1** and ATP. Upon doping of ATP into the solution of **1** in D_2O, the aromatic protons of **1** and ATP gradually shift upfield.

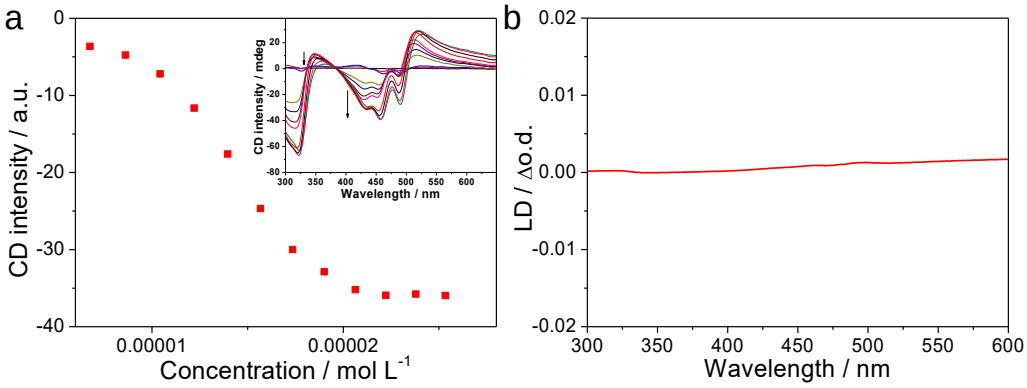

Supplementary Figure 20. (a) CD intensity changes at λ = 459 nm upon gradual addition of ATP into **1** (2.0×10^{-5} M). Inset of (a): CD spectra variations upon gradual addition of ATP into **1**. (b) LD signal of **1**/ATP (2.0×10^{-5} M) in HEPES buffer. Upon progressively adding ATP into **1**, the Cotton effect gradually appears, which indicates that ATP induces a preferred helical handedness to the resulting co-assembly of **1**/ATP. No LD signal can be observed for the co-assembly of **1**/ATP ([**1**] : [ATP] = 1 : 1). Therefore, the measured CD signals are real to reflect the supramolecular chirality, without the interference of LD.[4]

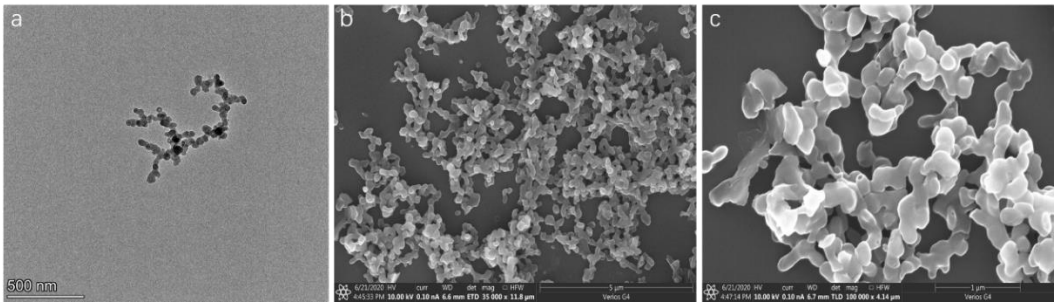

Supplementary Figure 21. (a) TEM and (b)−(c) micrographs of **1**/ATP ([**1**] : [ATP] = 1 : 1).

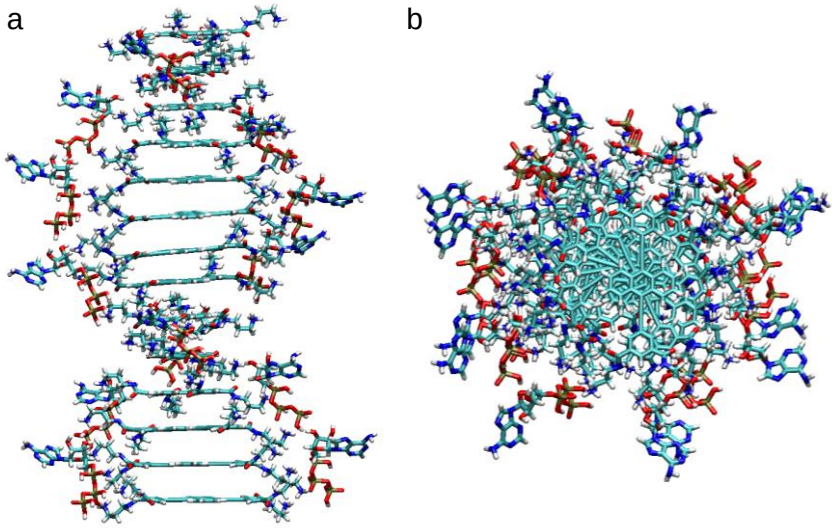

Supplementary Figure 22. (a) Side view and (b) top view of the structure of co-assembly **1**/ATP obtained from MD simulations at the initial snapshots.

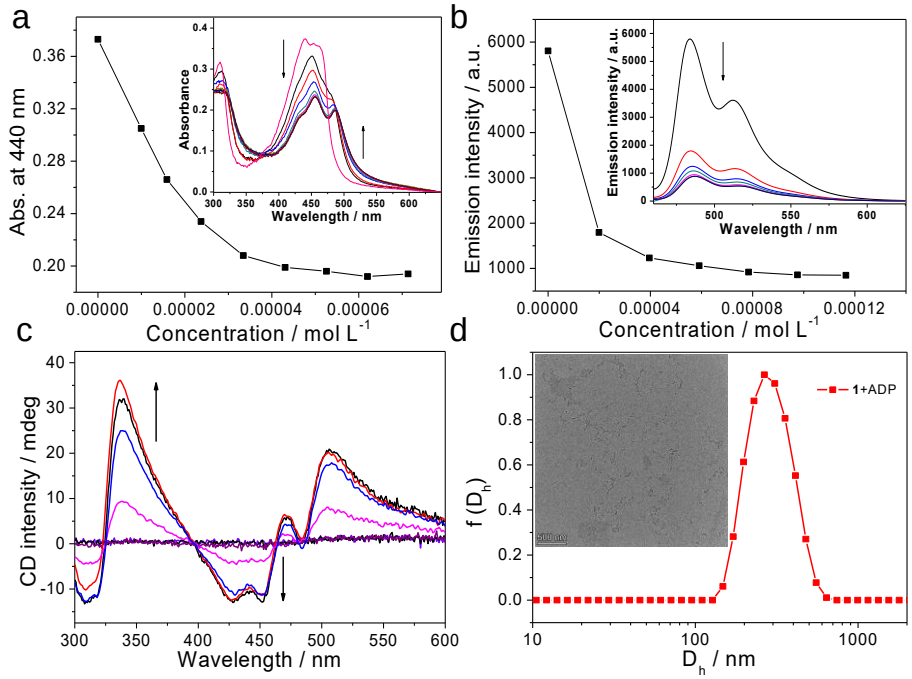

Supplementary Figure 23. (a) UV–Vis, (b) fluorescence, (c) CD, and (d) DLS spectra variations upon gradual addition of ADP into **1** (2.0×10^{-5} M in HEPES buffer). Specifically, around two equivalents of ADP are required to reduce the absorbance and emission intensities. Moreover, ADP can also induce CD signals with an isodichroic point at 397 nm, but less intense to that of ATP. Only small aggregations are formed for the resulting co-assembly **1**/ADP ([**1**] : [ADP] = 1 : 2), as evidenced by the TEM and DLS measurements.

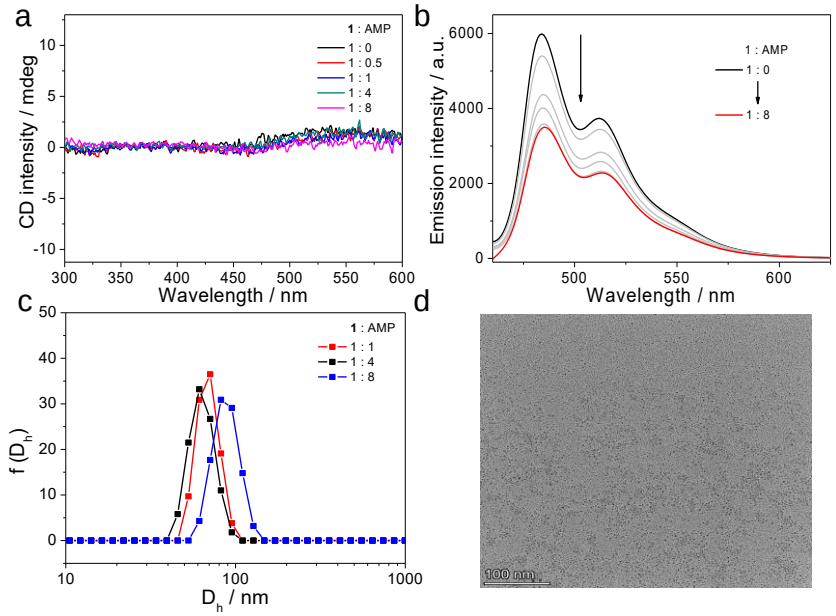

Supplementary Figure 24. (a) CD, (b) fluorescence, and (c) DLS spectra variations upon gradual addition of AMP into **1** (2.0×10^{-5} M in HEPES buffer). (d) TEM image of **1**/AMP ([**1**] : [ATP] = 1 : 8). Even though an excess of AMP is added into **1**, no apparent co-assembly can be observed.

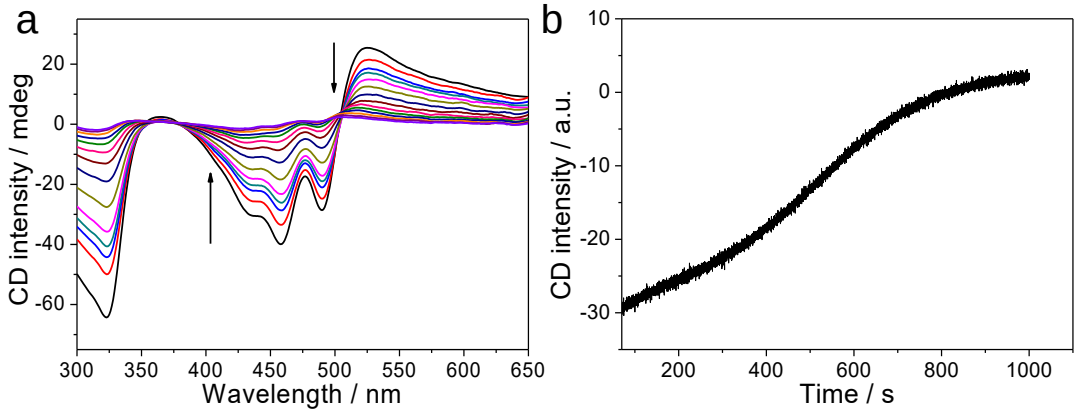

Supplementary Figure 25. (a) CD spectra variations of **1**/ATP *versus* hydrolysed time in the presence of 0.32 U mL^{-1} of ALP. (b) CD intensity of **1**/ATP at 510 nm as a function of time ([**1**] = 2.0×10^{-5} M, [ATP] = 2.0×10^{-5} M, aqueous HEPES buffer, pH = 7.0). Time-dependent CD spectra show a weakening trend during the enzymatic process of **1**/ATP by ALP, indicating the gradual disassembly of the chiral aggregates.

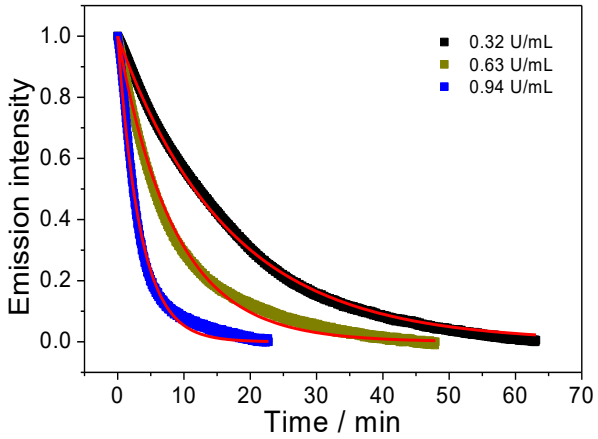

Supplementary Figure 26. Plot of time-dependent emission intensity monitored at 484 nm showing the disassembly process of **1**/ATP, with varying ALP concentration. The solid lines correspond to their first-order kinetic fits. Emission signals are normalized between zero and one for the ease of fitting into kinetic model. ([**1**] = 2.0×10^{-5} M, [ATP] = 2.0×10^{-5} M, aqueous HEPES buffer, pH = 7.0). When the amount of ALP increases from 0.32 U mL^{-1} *via* 0.63 U mL^{-1} to 0.94 U mL^{-1}, the recovery half-life time (defined as the time required to reach 50% of the fluorescence intensity) shortens from 14.5 min *via* 7.3 min to 3.6 min. The corresponding rate constants of disassembly are calculated to be 0.06 min^{-1}, 0.12 min^{-1}, and 0.29 min^{-1}.

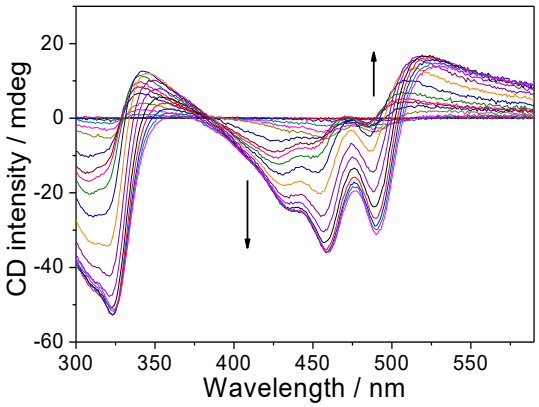

Supplementary Figure 27. CD spectra variations upon re-addition of ATP (2.0×10^{-5} M) into the mixture solution of **1**/ALP. The Cotton effects totally restore to the initial state as a function of time, which indicates the chiral co-assembly **1**/ATP is re-formed.

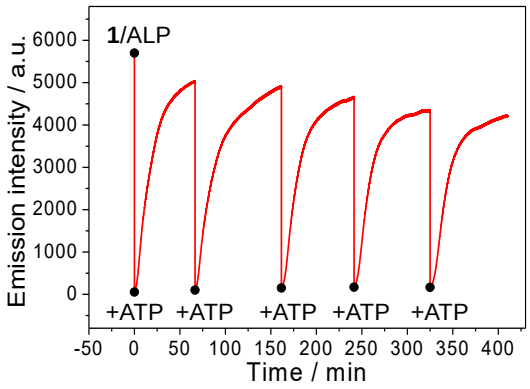

Supplementary Figure 28. Fluorescent intensity at 484 nm on several repetitive additions of ATP to **1** in the presence of 0.32 U mL^{-1} of ALP ([**1**] = 2.0 × 10^{-5} M, [ATP] = 2.0 × 10^{-5} M, aqueous HEPES buffer, pH = 7.0). With continuously adding new batches of ATP to **1** in the presence of ALP, the emission signal is reversibly switched for at least five cycles.

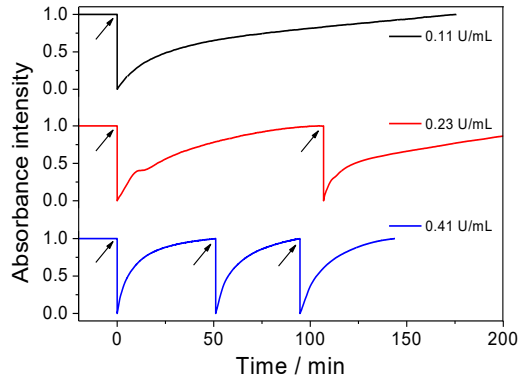

Supplementary Figure 29. Time-dependent absorbance intensity at 442 nm on several repetitive additions of ATP to **1** in the presence of 0.11 U mL^{-1}, 0.23 U mL^{-1}, and 0.41 U mL^{-1} of ALP, respectively. Arrows represent the (re)fueling points with the addition of ATP. ([**1**] = 2.0 × 10^{-5} M, [ATP] = 2.0 × 10^{-5} M, aqueous HEPES buffer, pH = 7.0).

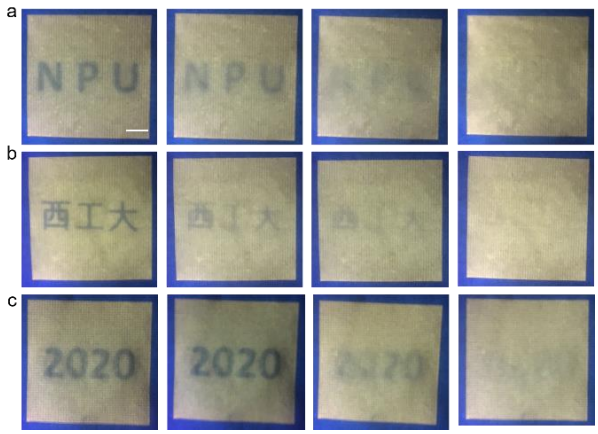

Supplementary Figure 30. Photographs of the printed patterns. The yellow emission background is printed with the aqueous solution of **1** as inks. (a) The "NPU" pattern that printed with the inks of ATP is gradually disappeared after spraying with ALP inks. (b) The reprinted pattern of Chinese characters with ATP inks at the same location of (a), is gradually disappeared after spraying with ALP inks. (c) The reprinted pattern of "2020" with ATP inks at the same location of (b), is gradually disappeared after spraying with ALP inks. Scale bar: 5 mm. Upon successively printing with ATP and spraying with ALP, the writing/erasing process can be proceeded for multiple times.

Supplementary Figure 31. Photographs of the printed patterns. The word of (a) "message" and (b) "Encoded Information" that handwritten with a fountain pen loaded with the ATP inks are gradually disappeared after spraying with ALP inks. Scale bar: 5 mm.

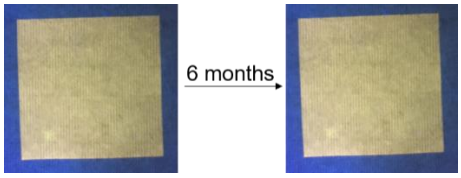

Supplementary Figure 32. Photographs of the printed yellow emission paper with the aqueous solution of **1** as inks on day 1 and after 6 months. The rewritable paper features enough stability under the atmosphere condition, as evidenced by the unchanging of the emission color for at least half a year.

Supplementary References:

1. Lebtow, M. *et al*. Self-Assembly of 9,10-Bis(phenylethynyl) Anthracene (BPEA) Derivatives: Influence of π–π and Hydrogen-Bonding Interactions on Aggregate Morphology and Self-Assembly Mechanism. *Chem. Eur. J.* **23**, 6198–6205 (2017).
2. Zhao, D., Yuan, D., Krishna, R., van Batenb, J. M. & Zhou, H.-C. Thermosensitive gating effect and selective gas adsorption in a porous coordination nanocage. *Chem. Commun.* **46**, 7352–7354 (2010).
3. Shao, K. *et al.* Tailoring the pore geometry and chemistry in microporous metal–organic frameworks for high methane storage working capacity. *Chem. Commun.* **55**, 11402–11405 (2019).
4. Norden, B. Linear and circular dichroism of polymeric pseudoisocyanine. *J. Phys. Chem.* **81**, 151–159 (1977).